Calculations of magnetic x-ray dichroism in the 3*d* absorption spectra of rare-earth compounds

J. B. Goedkoop
Research Institute of Materials, Faculty of Science, University of Nijmegen, Toernooiveld, 6525 ED Nijmegen, The Netherlands

B. T. Thole, G. van der Laan, and G. A. Sawatzky
Department of Applied and Solid State Physics, Materials Science Center, University of Groningen, Nijenborgh 18, 9747 AG Groningen, The Netherlands

F. M. F. de Groot and J. C. Fuggle
Research Institute of Materials, Faculty of Science, University of Nijmegen, Toernooiveld, 6525 ED Nijmegen, The Netherlands
(Received 13 April 1987)

We present atomic calculations for the recently discovered magnetic x-ray dichroism (MXD) displayed by the 3*d* x-ray-absorption spectra of rare-earth compounds. The spectral shapes expected at $T=0$ K for linear polarization parallel and normal to the local magnetic field is given, together with the temperature and field dependencies of the intensities of the spectral lines. It is concluded that strong MXD effects can be expected for all rare-earth ions except those having a ground state with either $J=0$ or $L=0$.

I. INTRODUCTION

In two short papers we have predicted[1] and confirmed[2] the existence of a strong polarization dependence of the 3*d* x-ray absorption spectra (XAS) of magnetically ordered rare-earth materials. We expect that this effect, magnetic x-ray dichroism (MXD), can be a useful probe of the orientation and size of local magnetic moments in rare earths, actinides, and possibly some transition-metal compounds. In such materials, where the open valence shells have predominantly atomic character, the *absolute value* of the local moment is approximately that of the free ion (i.e., no quenching of the orbital moment). Here the parameters of interest are the local magnetic field and the orientation of the ionic moment relative to the net magnetization. For example, most of the rare-earth metals have ordered magnetic structures in which the ionic moments form spirals along the direction of the net magnetization with a temperature-dependent pitch. In this paper we discuss the use of MXD to determine the temperature and field dependence of the orientation of the moment.

XAS in a total photoelectron yield mode is to some extent surface sensitive with a strongly material-dependent probing depth ranging from 50 to ~ 1000 Å. In our own experiments we have found that the surface layer of a rare-earth metal gives a signal $\geq 5\%$ of that from the bulk and the minimum detection limit is a fraction of a monolayer. Thus the MXD effect described here could be used to study thin-film and potentially surface magnetic structures. As it is described completely in terms of *local ionic moments,* it is complementary to other spectroscopies sensitive to surface magnetization such as spin-polarized photoemission, electron-capture spectroscopy (ECS), spin-polarized low-energy electron diffraction (SPLEED), etc., that yield data on the surface spin polarization and/or band structure of, e.g., V, Cr, Fe, Co, Ni metals, and thin films.

MXD effects have also been found in the *L*-edge spectra of Gd (Ref. 3) and the *K*-edge spectra of Fe (Ref. 4), but until now appear to be much weaker than those described here.

The origin of the MXD effect is basically quite simple but the atomic physics involved is usually not part of the knowledge of solid-state physicists. In this paper we therefore start with a short introduction to nonmagnetic $3d \rightarrow 4f$ absorption spectra of rare-earth materials and illustrate the physics of the MXD effect on the basis of the very simple case of Yb^{3+}. Subsequently, a more exact theoretical description is given, followed by an evaluation of calculated MXD spectra for linear polarized x rays.

II. 3*d* XAS OF RARE-EARTH MATERIALS

The distinguishing feature of the rare-earth elements in solids is the atomic character of the 4*f* levels, which lie relatively deep in the ion while having very small binding energies. It is this feature that accounts for the chemical similarity and magnetic diversity found in the series. A well-known consequence of this localized behavior is that a number of solid-state and gas-phase spectroscopies involving the 4*f* electrons can be explained with the multiplet structure found from atomic calculations, with only small corrections being necessary to incorporate solid-state effects. This holds even for high-energy spectroscopies such as $3d \rightarrow 4f$ XAS,[5–8] where the predictive power of the atomic model is even

sufficient to use XAS as a probe of ground-state effects like the relative occupation of spin-orbit-split ground-state levels,[9] homogeneous[10–13] and heterogeneous valency mixing,[14] and, as was shown in Refs. 1 and 2, of magnetization. This is a somewhat surprising situation, as the energy scale of these effects (1–10 meV) is very small compared to the experimental resolution (~300 meV), the core-hole lifetimes [400–800 meV (Refs. 8 and 15)], and the photon energy (~keV) applicable to high-resolution XAS. All these possibilities are due to the amount of structure in the spectra, which in turn is a result of the spin-orbit splitting of the $3d$ hole, the strong Coulomb and exchange interaction of the $3d$ and $4f$ electrons, and the optical dipole selection rules.

In the upper panels of Fig. 1 we reproduce the calculated $3d$ absorption spectra of trivalent rare-earth ions.[16,17] The absorption process involves the electronic excitation

$$3d^{10}4f^n\,|\,\alpha JM\rangle \rightarrow 3d^9 4f^{n+1}\,|\,\alpha' J' M'\rangle\ ,$$

where all other shells are either filled or empty and α labels all other quantum numbers aside from J and M needed to specify the levels of the initial- and final-state multiplets. The final-state configuration contains two open shells and consequently forms a complex multiplet that in some cases consists of several thousands of levels $|\,\alpha' J' M'\rangle$, divided into two groups by the strong $3d$ spin-orbit interaction, which to a first approximation may be labeled $3d_{3/2}$ and $3d_{5/2}$. Of this multitude of states, only those that can be reached from the (Hund's rule) ground state $|\,\alpha JM\rangle$ under the optical selection rules $\Delta J = 0, \pm 1$ are present in the absorption spectrum. Transitions to the unoccupied $5p$ continuum states are also allowed but have near the absorption edge a negligible cross section compared to the $3d \rightarrow 4f$ transitions. In a more exact manner, the cross section of the absorption $|\,\alpha JM\rangle \rightarrow |\,\alpha' J' M'\rangle$ is described by[16]

$$S^m_{\alpha JM\alpha' J' M'} \propto \begin{pmatrix} J & 1 & J' \\ M & m & -M' \end{pmatrix}^2 |\,\langle \alpha J \| C^{(1)} \| \alpha' J' \rangle\,|^2 \ . \quad (1)$$

The first term on the right-hand side is the square of the 3-j symbol which dictates the distribution of the line strength $|\,\langle \alpha J \| C^{(1)} \| \alpha' J' \rangle\,|^2$ of an $\alpha J \rightarrow \alpha' J'$ transition over its different $M \rightarrow M'$ components. The 3-j symbol is nonzero only if $\Delta J = J' - J = 0, \pm 1$ ($J = J' = 0$ excluded) and $m \equiv \Delta M = M' - M = 0, \pm 1$ where $\Delta M = 0$ is possible only if the light is linearly polarized parallel to the z axis and $\Delta M = +1$ (-1) only if the light is (counter)clockwise circularly polarized in the (x,y) plane.

In the middle panels of Fig. 1 the same spectra are presented again, now with the vertical scale of the $3d_{3/2}$ group expanded. Here we have separated the spectra in the three contributions formed by the selection rules $\Delta J = 0, \pm 1$. Note that for most of the rare earths these contributions are readily distinguishable; in particular, in the $3d_{3/2}$ group of the early rare earths and in the $3d_{5/2}$ group of the late rare earths. Clear exceptions are found in the spectra of ions with a $J = 0$ ground state [$La^{3+}(f^0)$ and $Eu^{3+}(f^6)$], where $\Delta J = 1$ is the only available channel and $Gd^{3+}(f^7)$, where $L = 0$ and the ΔJ groups overlap in energy. In the other elements it is this distinguishability that allows for the detection of magnetic dichroism effects, because, as will be seen below, each ΔJ group turns out to have its own dependence on polarization, magnetization, and temperature.

The above considerations can be extended to include rare-earth ions with other valencies, since the shape of the multiplet is almost entirely determined by the number of f electrons. Thus, for instance, Eu^{2+} and Tb^{4+} have the same multiplet spectrum as Gd^{3+} since all have a $4f^7$ configuration.

III. MAGNETIC DICHROISM IN X-RAY ABSORPTION SPECTRA

A. The Yb^{3+} spectrum

Before giving the exact equations we will give a qualitative picture of the origin of the MXD effects based on the very simple absorption spectrum of Yb^{3+}, which consists of just one $\Delta J = -1$ line: $3d^{10}4f^{13}(^2F_{7/2}) \rightarrow 3d^9 4f^{14}(^2D_{5/2})$ (see Fig. 2). In the presence of a magnetic field H parallel to the z axis both the initial and the final states are split up into their Zeeman components with energies $-g\mu_B HM$, as depicted in the right-hand side of Fig. 2. One sees that the originally 18-fold degenerate $\Delta J = -1$ line consists of three groups of lines with equal ΔM. The dots below these lines indicate their relative amplitudes as given by the square of the 3-j symbol. If all Zeeman states are equally populated, i.e., at high temperatures, then the three groups will have equal contributions to the absorption cross section. In this situation no effect of the magnetic field will be present in the XAS spectrum, as the magnetic splitting is much smaller (~1 meV) than the experimental linewidth

However, the occupation of the levels M of the initial state is governed by a Boltzmann distribution $\exp(-M/\Theta)$, where Θ is the reduced temperature $kT/g\mu_B H$. If $\Theta \gg 1$ the levels will be evenly occupied, but at lower values of Θ the upper levels will become depopulated and the absorption by these levels will diminish. As can be seen from the diagram, this causes the absorption strength of the different ΔM groups to become unequal resulting in different absorption coefficients for different polarizations. This is most clearly demonstrated in the limit of $T = 0$ K where only the $M = -\frac{7}{2}$ level is occupied, so that the $\Delta M = 1$ transition indicated by the solid arrow in Fig. 2 is the only possible transition. Consequently, the Yb absorption line is seen to be absent at $T = 0$ K both for clockwise circular polarization normal to H as well as for linear polarization parallel to H. This behavior is typical for a $\Delta J = -1$ line. A similar mechanism acts on $\Delta J = 0$ and $\Delta J = 1$ lines, but leads to other dependencies on Θ, as will be discussed below.

B. General theory

The general expression for the cross section in the presence of a magnetic field H is obtained by taking the Boltzmann weighted average of Eq. (1):

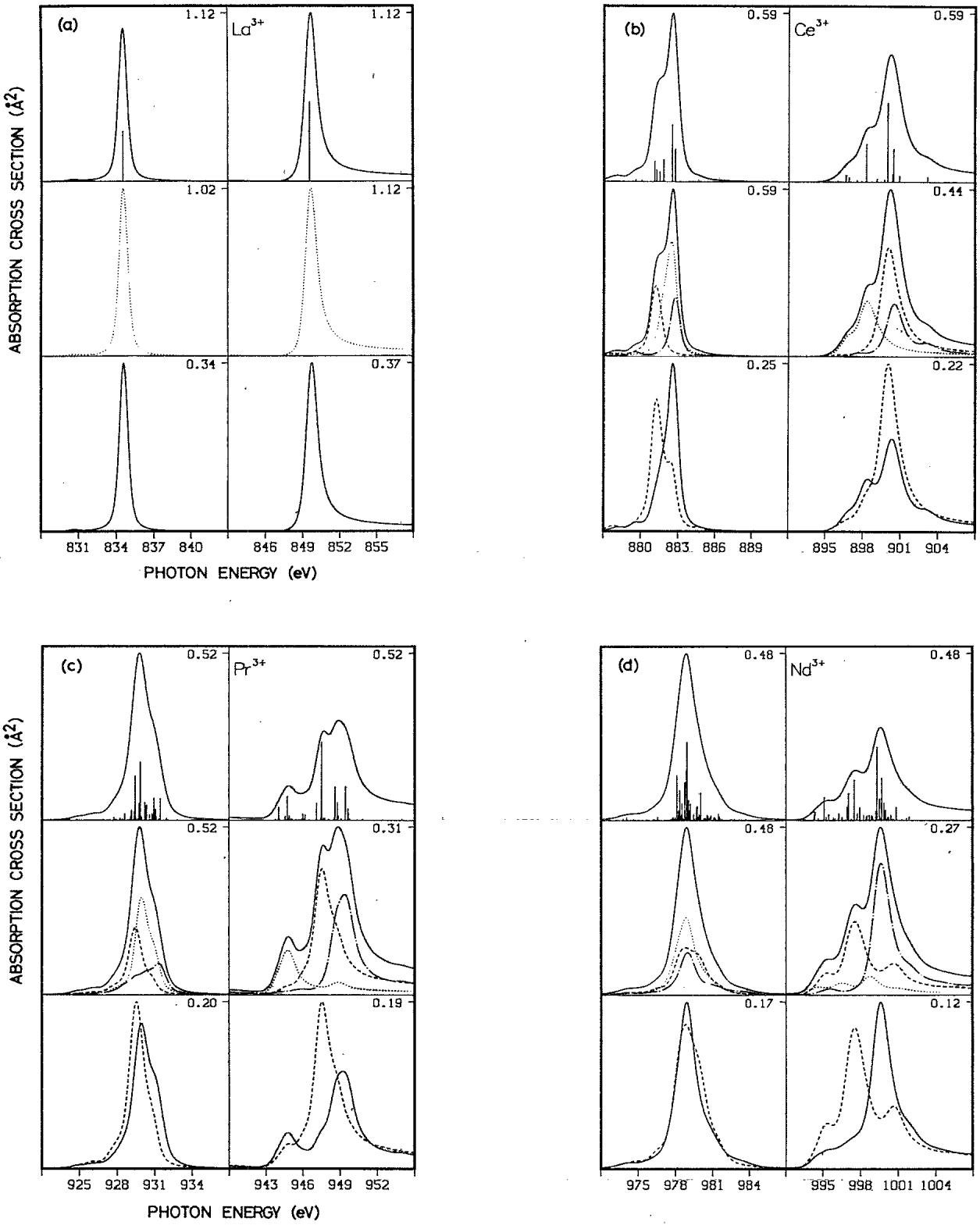

FIG. 1. Upper panels: calculated $3d \rightarrow 4f$ x-ray absorption spectra of trivalent rare-earth ions. The curves denote the absorption cross section of the $3d_{5/2}$ (left) and $3d_{3/2}$ (right) groups in units of Å^2. They were derived from the oscillator strengths (plotted as vertical bars with arbitrary scale) by convolution with lines representing the lifetime of the $3d$ hole and the instrumental broadening (Ref. 17). Horizontal scale: excitation energy (eV). Middle panels: the same curves with the vertical scale of the $3d_{3/2}$ part expanded showing the contribution of each ΔJ group to the total spectrum. —·—·—·, $\Delta J=-1$; — — —, $\Delta J=0$; · · · ·, $\Delta J=+1$. Since the La^{3+}, Eu^{3+}, and Yb^{3+} spectra contain only one contribution, the total spectrum coincides with the dashed line and therefore has been left out. Lower panels: Calculated cross section at $T=0$ K with polarization parallel (— — —) and perpendicular (——) to the internal magnetic field.

$$S^m_{\alpha JM\alpha' J'M'}(\Theta) \propto A^m_{JJ'}(\Theta)\,|\,\langle \alpha J\|C^{(1)}\|\alpha' J'\rangle\,|^2\,, \qquad (2)$$

where

$$A^m_{JJ'}(\Theta)=\frac{\sum_{M=-J}^{J}\begin{bmatrix} J & 1 & J' \\ M & m & -M' \end{bmatrix}^2 e^{-M/\Theta}}{\sum_{M=-J}^{J} e^{-M/\Theta}}\,. \qquad (3)$$

For each of the nine allowed combinations of ΔJ and ΔM this can be rewritten in terms of J, $\langle M\rangle$, and $\langle M^2\rangle$ (see Table I). Since[18]

$$\langle M\rangle = -JB_J\left[\frac{J}{\Theta}\right], \qquad (4)$$

$$\langle M^2\rangle = J(J+1)+\langle M\rangle \coth\left[\frac{1}{2\Theta}\right], \qquad (5)$$

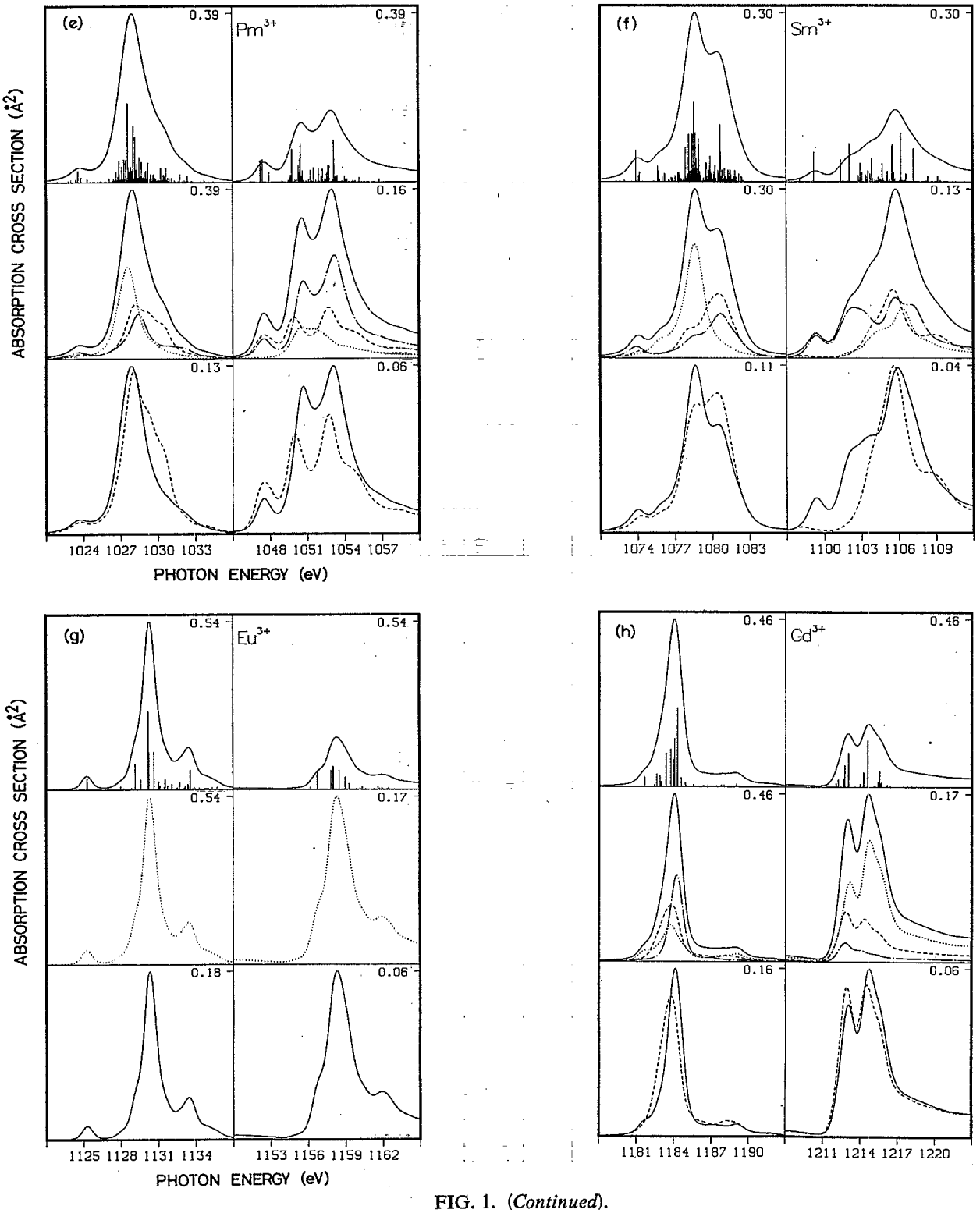

FIG. 1. (*Continued*).

where $B_J(J/\Theta)$ is the Brillouin function, it follows that the $A^m_{JJ'}(\Theta)$ are functions of J and Θ only.

IV. MXD SPECTRA FOR LINEARLY POLARIZED RADIATION

At present the only available source of intense tunable monochromatic radiation in the soft-x-ray range is a synchrotron equipped with a double-crystal monochromator. This source is linearly polarized with the E vector in the plane of the electron orbit.[19] Thus it is only possible to discriminate between cases where the polarization vector **E** is parallel to (**E**∥**H**) or normal to (**E**⊥**H**) the field. In the latter case, radiation can be decomposed in two circularly polarized components, with opposite senses of rotation, resulting in

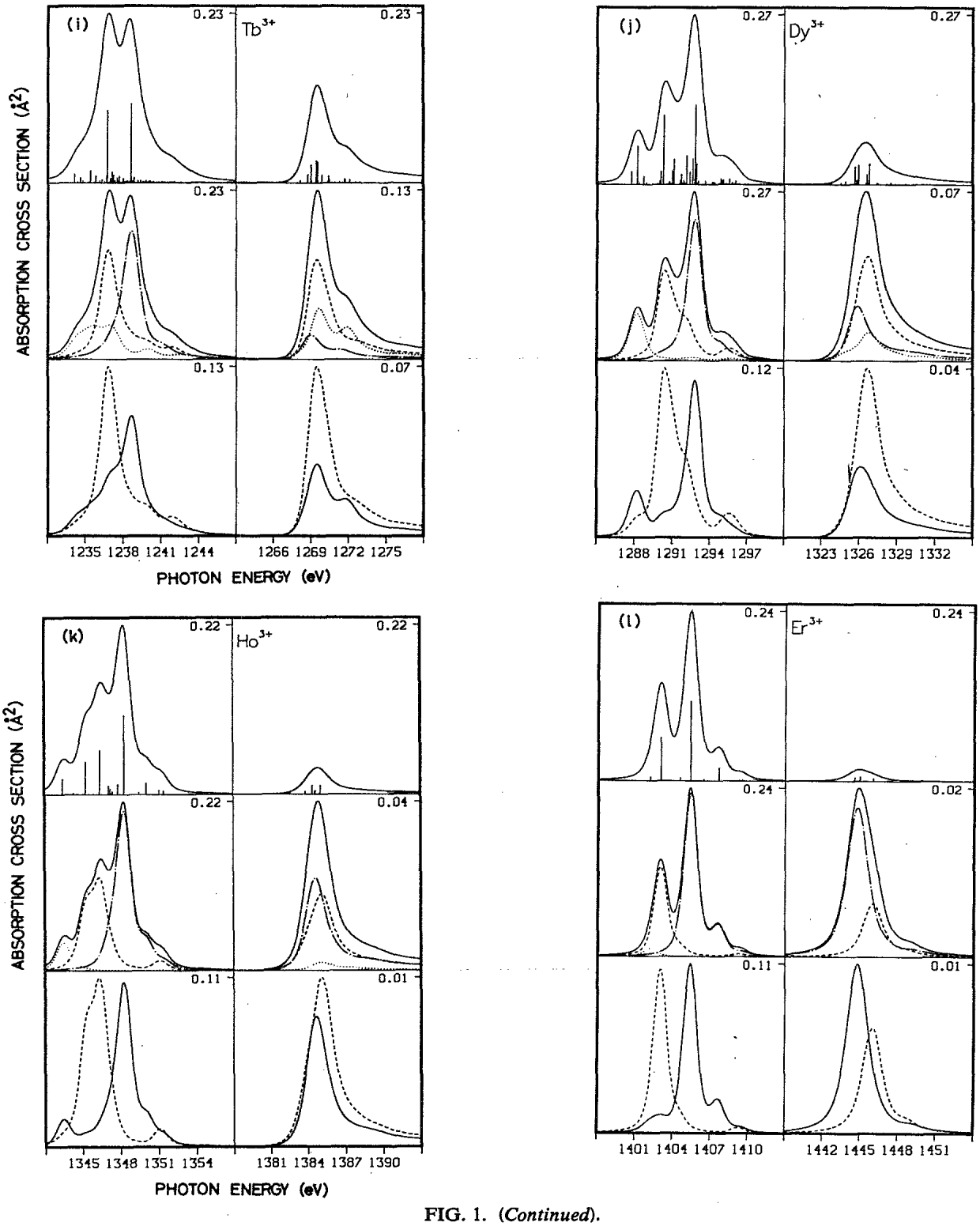

FIG. 1. (*Continued*).

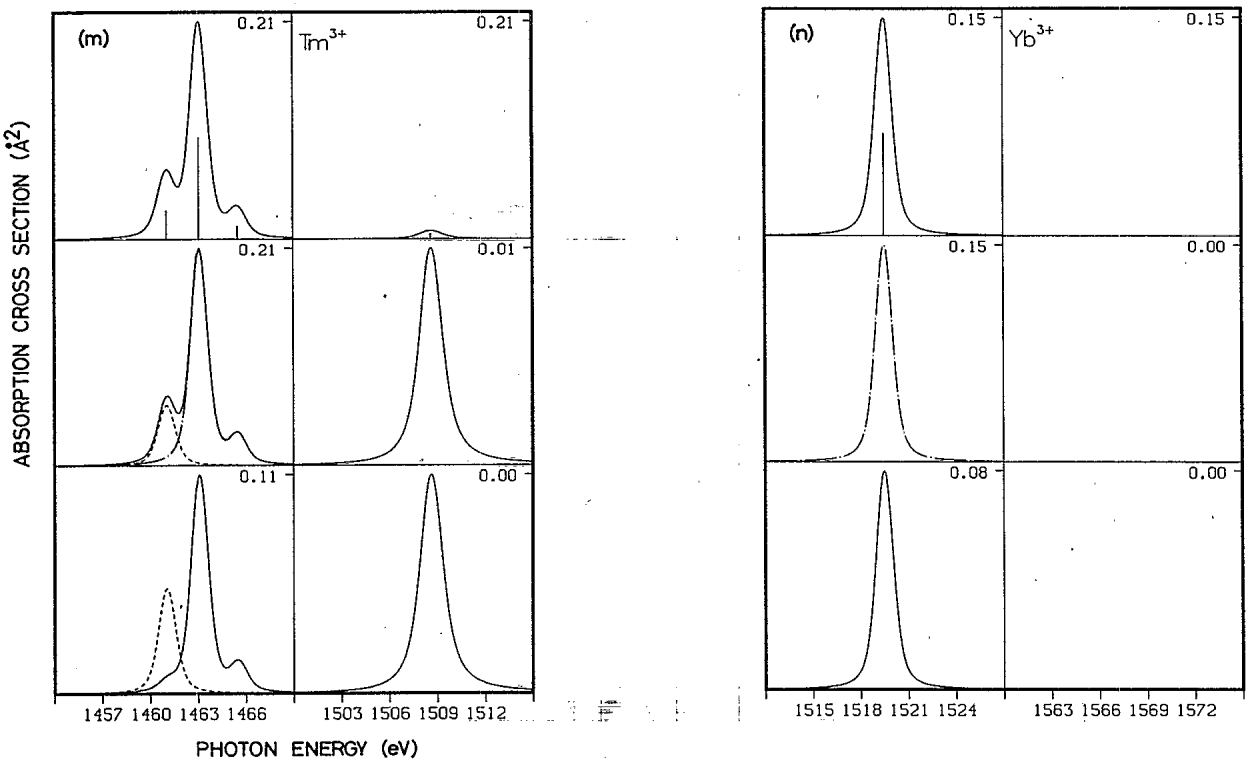

FIG. 1. (*Continued*).

$$A^{\parallel}_{JJ'}(\Theta)=A^{0}_{JJ'}(\Theta)\,,$$

$$A^{1}_{JJ'}(\Theta)=\frac{1}{2}[A^{-1}_{JJ'}(\Theta)+A^{+1}_{JJ'}(\Theta)] \tag{6}$$

$$=\frac{1}{2}\left[\frac{1}{2J+1}-A^{0}_{JJ'}(\Theta)\right],$$

and at intermediate angles γ the strength of a given $J\rightarrow J'$ line is dependent on Θ only through $A^{0}_{JJ'}(\Theta)$:

$$S^{\gamma}_{\alpha JM\alpha' J'M'}(\Theta)\propto\left[A^{0}_{JJ'}(\Theta)\cos^2\gamma+\frac{1}{2}\left[\frac{1}{2J+1}-A^{0}_{JJ'}(\Theta)\right]\sin^2\gamma\right]\times|\langle\alpha J\|C^{(1)}\|\alpha' J'\rangle|^2\,. \tag{7}$$

For the trivalent rare-earth ions we need to evaluate $A^{0}_{JJ'}(\Theta)$ only for $J=\frac{5}{2}$ (Ce,Sm), $\frac{7}{2}$ (Gd,Yb), 4 (Pr,Pm), $\frac{9}{2}$ (Nd), 6 (Tb,Tm), $\frac{15}{2}$ (Dy,Er), and 8 (Ho). For these values of J the curves for $(2J+1)A^{0}_{JJ'}(\Theta)$ (Table I) are drawn in Fig. 3. At high temperatures the intensity of each of the ΔJ channels has the statistical value $1/3(2J+1)$. On lowering Θ the magnetic moment starts to align itself parallel to the effective magnetic field [Eq. (4)], affecting the amplitude of each ΔJ line in the manner described above. From the curves, one sees that the MXD effects become important for $\Theta\lesssim 3$, the earlier so for larger ground-state J values. At $T=0$ the $\Delta J=-1$ lines indeed disappear as expected from the discussion of Yb while the $\Delta J=0$ and 1 amplitudes remain finite with a value given by Eq. (1) with $M=J$ and $M'=-(J+\Delta J)$.

In order to give an impression of the extent of the effect at $\Theta=0$, we reproduce in the lower panels of Fig. 1 the MXD spectra of (hypothetically) ferromagnetic ordered trivalent rare-earth ions for parallel and perpendicular polarizations [Eq. (6)]. From these curves it is clear that a strong linear dichroism can be expected in nearly all cases. Magnetic effects are clearly absent in La^{3+} and Eu^{3+} because these ions have a $J=0$ ground state. $Gd^{3+}(4f^7)$ has an $L=0$ ground state, causing, as

TABLE I. The expressions for the factors $A^{m}_{JJ'}$ giving the intensity of $\Delta J=-1$, 0, and 1 lines for different polarization states of the light with respect to the local magnetic moment $\langle M\rangle$.

	$m=0$	$m=\pm 1$
A^{m}_{JJ+1}	$\dfrac{(J+1)^2-\langle M^2\rangle}{(2J+3)(J+1)(2J+1)}$	$\dfrac{(J+1)(J+2)\pm(2J+3)\langle M\rangle+\langle M^2\rangle}{2(2J+3)(J+1)(2J+1)}$
A^{m}_{JJ}	$\dfrac{\langle M^2\rangle}{J(J+1)(2J+1)}$	$\dfrac{J(J+1)\mp\langle M\rangle-\langle M^2\rangle}{2J(J+1)(2J+1)}$
A^{m}_{JJ-1}	$\dfrac{J^2-\langle M^2\rangle}{J(2J-1)(2J+1)}$	$\dfrac{J(J-1)\mp(2J-1)\langle M\rangle+\langle M^2\rangle}{2J(2J-1)(2J+1)}$

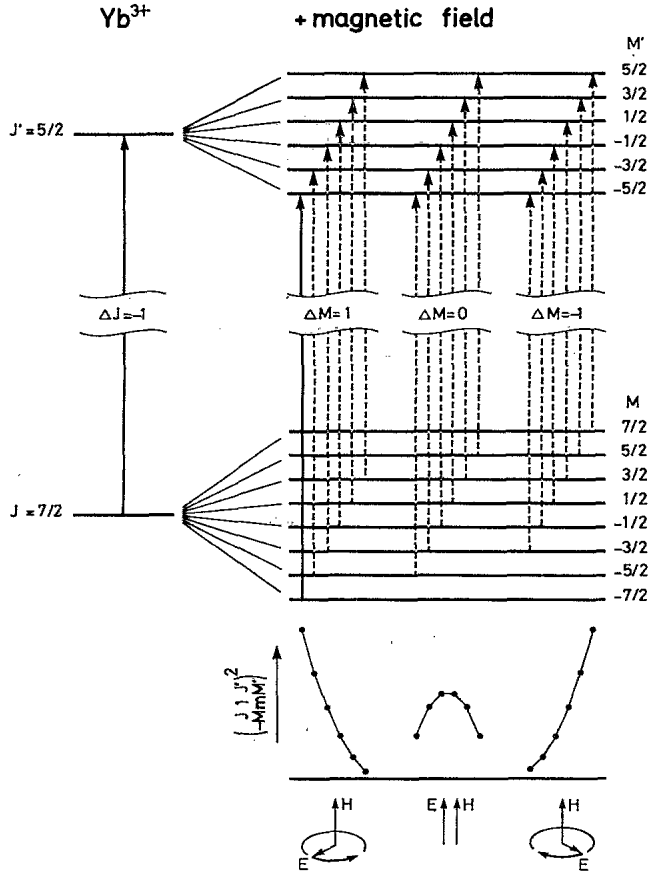

FIG. 2. Energy-level diagram of the $3d^{10}4f^{13} \rightarrow 3d^9 4f^{14}$ transition of Yb^{3+} without (left) and with (right) a magnetic field. The transitions $|JM\rangle \rightarrow |J'M'\rangle$ that are allowed by the optical dipole selection rules are indicated by the arrows. Their relative intensities are given by the dots. The polarization of the light with respect to the magnetic field **H** required for the different ΔM channels is indicated at the bottom. As described in the text, only the $M = -\frac{7}{2} \rightarrow M' = -\frac{5}{2}$ line of the $\Delta M = 1$ channel indicated by the solid arrow is allowed at 0 K.

noted above, an overlap in energy position of the three ΔJ contributions. For the same reasons MXD effects are absent in Ce^{4+}, Sm^{2+}, and Yb^{2+} ($J=0$) and small in Eu^{2+} and Tb^{4+} ($L=0$).

For the remaining elements the effects are especially strong in the $3d_{3/2}$ region of Ce^{3+}, Pr^{3+} (Ce^{2+}), and Nd^{3+} and in the $3d_{5/2}$ region of Tb^{3+}, Dy^{3+}, Ho^{3+}, Er^{3+}, Tm^{3+}, and Yb^{3+}. For Sm^{3+}, MXD effects should be strong but the situation is complicated by the poorer agreement between the Sm^{3+} $3d_{3/2}$ spectra calculated in the atomic model and that observed experimentally.[8]

Since the shape of the spectra is dependent on the *size* and *orientation with respect to the polarization* of the ionic moment [see Eq. (7)], MXD spectra can be used to obtain information thereon. With linear polarized light the *direction* of the moment along the axis cannot be extracted. The requisite dependence on $\langle M \rangle$ is present only in the expressions for $A_{JJ'}^{+1}$ and $A_{JJ'}^{-1}$ which implies the use of circular polarized light.

When there is no strict ferromagnetic ordering of the moments, the spectrum is a superposition of the spectra of the individual ions. This situation always leads to a reduction of the effect, as was discussed for the terbium iron garnet in Ref. 2.

V. CONCLUSIONS

We have presented predictions for the magnetic dichroism expected in the $3d$ x-ray absorption spectra of trivalent rare-earth ions based on atomic calculations. Nearly all cases show strong MXD effects with linear polarization. No effect is predicted for La^{3+} and Eu^{3+} and for the ions with the same configurations Ce^{4+}, Sm^{2+}, Yb^{2+} because these ions have a $J=0$ ground state.

Gd^{3+} and Eu^{2+} unfortunately form the exceptions of the series. Because of the $L=0$ ground state the ΔJ groups are overlapping, resulting in only small MXD effects in these magnetically important elements. For

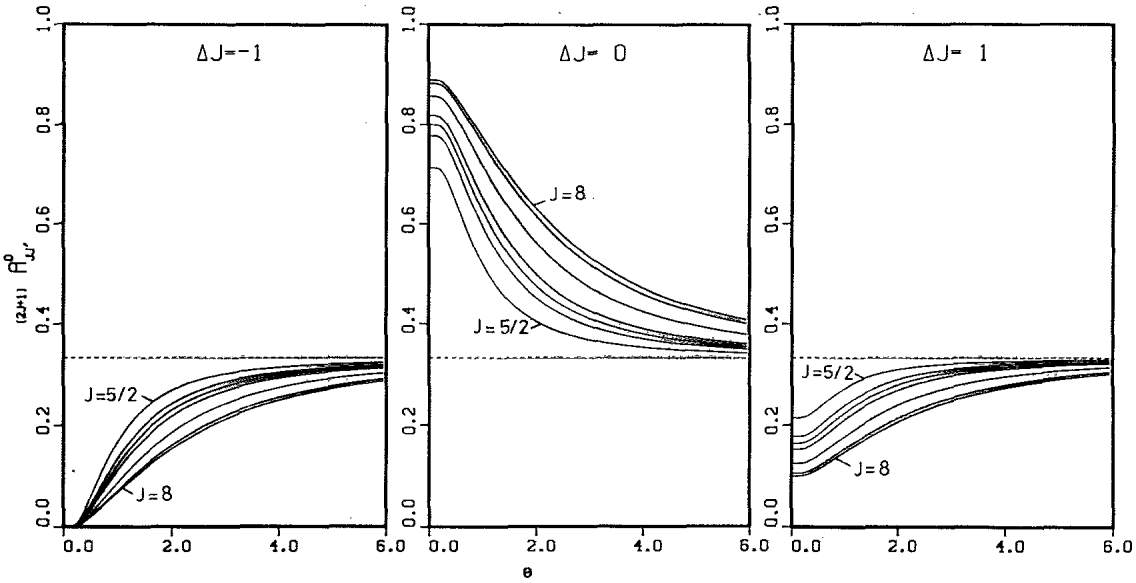

FIG. 3. Plot of the intensity $A_{JJ'}^0(\Theta)$ for $J'-J=-1$, 0, and 1 normalized to $2J+1$ as a function of the reduced temperature Θ. From the dashed line outwards: $J=\frac{5}{2}$, $\frac{7}{2}$, 4, $\frac{9}{2}$, 6, $\frac{15}{2}$, and 8.

the remaining trivalent elements and Ce^{2+} the effects are especially large in the $3d_{3/2}$ region for the first half of the series and in the $3d_{5/2}$ region for the second half of the series. With linearly polarized light, MXD measurements as a function of magnetic field and temperature can be expected to yield data on the axis of magnetic ordering and on the value of $\langle M^2 \rangle$.

We did not discuss the use of circular polarization in detail because of the present lack of suitable sources, but calculations show the effects to be somewhat stronger in this case. Also we note the use of circular polarized light would make MXD sensitive to the sign of $\langle M \rangle$ along the axis of ordering. Finally, the MXD effect can be used in principle for the production of circular polarization at some discrete absorption energies by filtering out one of the circular components of a linear polarized beam, much in the way a Pockel cell is used for visible wavelengths.

ACKNOWLEDGMENTS

This work was supported in part by the Netherlands Foundation for Chemical Research (SON) with financial support from the Netherlands Organization for the Advancement of Pure Research (ZWO) and by the Committee for the European Development of Science and Technology (CODEST) program. A NATO travel grant was very useful and is gratefully acknowledged.

[1]B. T. Thole, G. van der Laan, and G. A. Sawatzky, Phys. Rev. Lett. **55**, 2086 (1985).

[2]G. van der Laan, B. T. Thole, G. A. Sawatzky, J. B. Goedkoop, J. C. Fuggle, J.-M. Esteva, R. C. Karnatak, J. P. Remeika, and H. A. Dabkowska, Phys. Rev. B **34**, 6529 (1986).

[3]E. Keller and E. A. Stern, *EXAFS and Near Edge Structure III* (Springer-Verlag, Berlin, 1984), p. 507.

[4]G. Schütz, W. Wagner, W. Wilhelm, P. Kienle, R. Zeller, R. Frahm, and G. Materlik, Phys. Rev. Lett. **58**, 737 (1987).

[5]J. Sugar, Phys. Rev. A **6**, 1764 (1972); Phys. Rev. B **5**, 1785 (1972); J. Sugar, W. P. Brewer, G. Kalkowski, G. Kaindl, and E. Paparazzo, Phys. Rev. A **32**, 2242 (1985).

[6]C. Bonelle, R. C. Karnatak, and J. Sugar, Phys. Rev. A **9**, 1920 (1974); C. Bonelle, R. C. Karnatak, and N. Spector, J. Phys. B **10**, 795 (1977).

[7]S. A. Yavna, V. L. Sukhorukov, and V. F. Demekhin, Fiz. Tverd. Tela (Leningrad) **26**, 2300 (1984) [Sov. Phys.—Solid State **26**, 1396 (1984)]; V. F. Demekhin, *ibid.* **16**, 1020 (1974) [*ibid.* **16**, 659 (1974)].

[8]B. T. Thole, G. van der Laan, J. C. Fuggle, G. A. Sawatzky, R. C. Karnatak, and J.-M. Esteva, Phys. Rev. B **32**, 5107 (1985).

[9]G. van der Laan, B. T. Thole, G. A. Sawatzky, J. C. Fuggle, J.-M. Esteva, R. C. Karnatak, and B. Lengeler, J. Phys. C **19**, 817 (1986).

[10]O. Gunnarsson, K. Schönhammer, J. C. Fuggle, F. U. Hillebrecht, J.-M. Esteva, R. C. Karnatak, and B. Hillebrand, Phys. Rev. B **28**, 7330 (1983); J. C. Fuggle, F. U. Hillebrecht, J.-M. Esteva, R. C. Karnatak, O. Gunnarsson, and K. Schönhammer, *ibid.* **27**, 4637 (1983); J. C. Fuggle, Physica **130**, 56 (1985), and references therein.

[11]O. Gunnarsson and K. Schönhammer, J. Magn. Magn. Mater. **52**, 141 (1985).

[12]T. Jo and A. Kotani, J. Phys. Soc. Jpn. **55**, 2457 (1986).

[13]J. W. Allen, S. J. Oh, O. Gunnarsson, K. Schönhammer, M. P. Maple, M. S. Torikachvili, and I. Lindau, Adv. Phys. **35**, 275 (1986).

[14]G. van der Laan, J. C. Fuggle, M. P. van Dijk, A. J. Burggraaf, J.-M. Esteva, and R. C. Karnatak, J. Phys Chem. Solids **47**, 413 (1986).

[15]J. C. Fuggle and S. F. Alvarado, Phys. Rev. A **22**, 1615 (1980).

[16]R. D. Cowan, *The Theory of Atomic Structure and Spectra* (University of California Press, Berkeley, 1981).

[17]The spectra in Fig. 1 were calculated in intermediate coupling with an atomic Hartree-Fock program with relativistic corrections (see Ref. 16). The single-configuration exchange and Coulomb integrals were scaled to 80% of their Hartree-Fock value. The solid curves were derived from the oscillator strengths (bars) by convolution with Lorentz ($3d_{5/2}$) and Fano ($3d_{3/2}$) lines representing the lifetime broadening of the $3d$ hole (400–800 meV) and a Gaussian representing the experimental resolution (250–400 meV). Details of the calculations used here, together with a comparison with experimental XAS spectra of all the rare-earth metals have been described in Ref. 8.

[18]C. Kittel, *Introduction to Solid State Physics*, 5th ed. (Wiley, New York, 1976), p. 440.

[19]Undulators and wigglers producing circular by polarized light are under study; see, e.g., J. Goulon, P. Elleaume, and D. Raoux, Nucl. Instrum. Methods A **254**, 192 (1987), and references therein.